Volume 57
Number 29
14 April 2021
Pages 3523–3620

# ChemComm

Chemical Communications

rsc.li/chemcomm

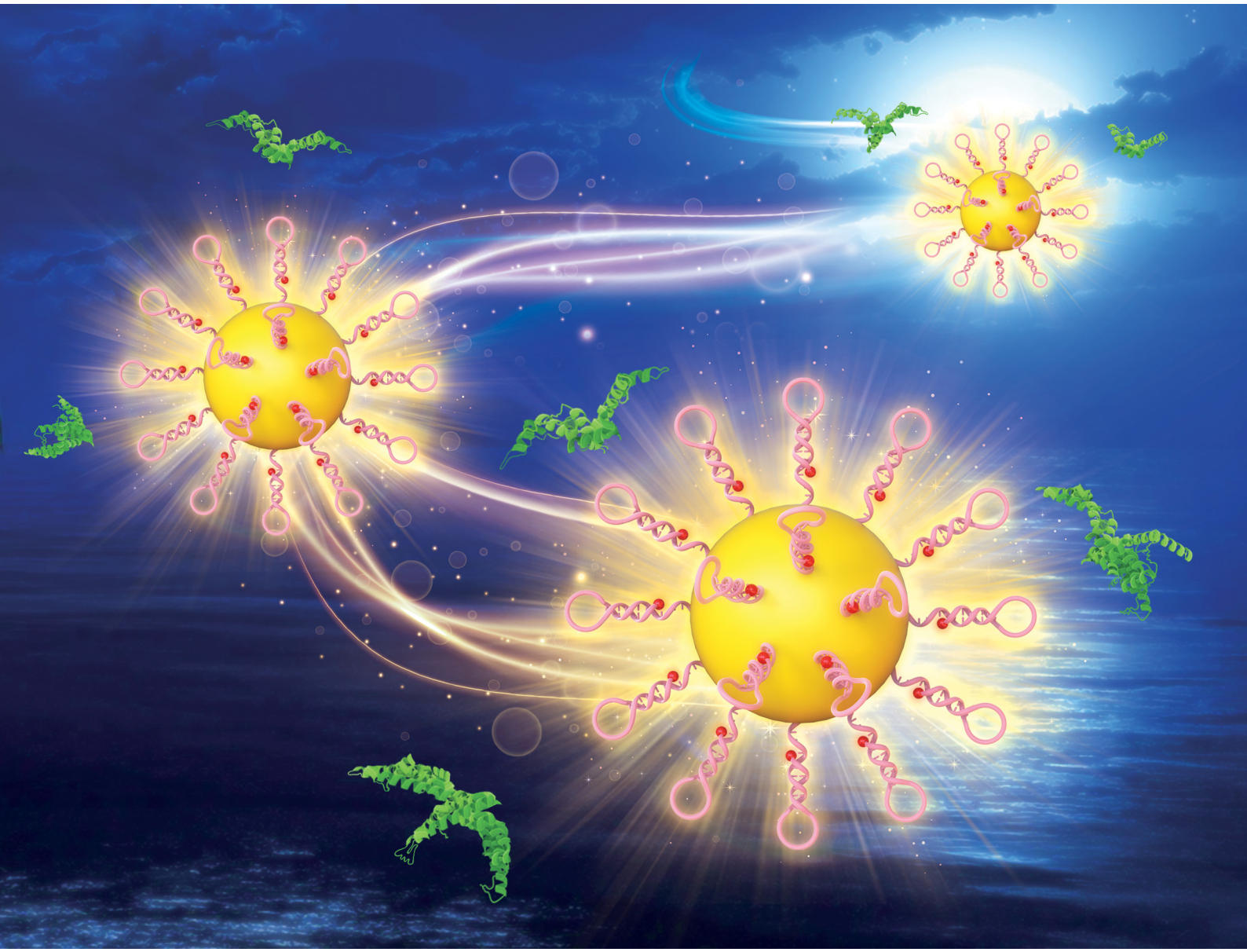

ISSN 1359-7345

ROYAL SOCIETY OF CHEMISTRY

**COMMUNICATION**

Jian-Ge Qiu, Chun-yang Zhang *et al.*

A single quantum dot-based fluorescence resonance energy transfer biosensor for antibody-free detection of ten-eleven translocation 1

ChemComm

COMMUNICATION

View Article Online
View Journal | View Issue

Check for updates

Cite this: *Chem. Commun.*, 2021, **57**, 3543

Received 24th February 2021,
Accepted 19th March 2021

DOI: 10.1039/d1cc01057c

rsc.li/chemcomm

Published on 19 March 2021. Downloaded on 5/15/2021 9:14:33 PM.

# A single quantum dot-based fluorescence resonance energy transfer biosensor for antibody-free detection of ten-eleven translocation 1†

Juan Hu,‡[ab] Jie Yao,‡[a] Jufeng Wang,‡[c] Li-yuan Pan,[a] Jian-Ge Qiu*[d] and Chun-yang Zhang *[a]

**We developed a single quantum dot-based fluorescence resonance energy transfer biosensor for antibody-free detection of ten-eleven translocation 1 (TET1). This biosensor can sensitively detect TET1 in a homogeneous manner without the involvement of any specific antibodies, and it can be used for accurate measurement of TET1 activity in human neuroblastoma cells and the screening of TET1 inhibitors.**

DNA demethylation plays critical roles in many biological processes including epigenetic reprogramming, regulation of gene expression, neurogenesis, and differentiation.[1] TET1 is an Fe(II)- and 2-oxoglutarate-dependent dioxygenase responsible for DNA 5-methylcytosine (5mC) demethylation in mammals.[2] TET1 can catalyze the conversion of 5mC to 5-hydroxymethylcytosine (5hmC) by transferring one oxygenic atom from an oxygen molecule to the C5-methyl of 5mC.[3] TET1 can induce the iterative oxidation of 5mC,[4] and the resultant oxidized derivatives of cytosine can be recognized and removed by thymine DNA glycosylase to yield abasic sites.[5] The subsequent repair of abasic sites by the base excision repair pathway can restore unmethylated cytosine, leading to active cytosine demethylation in mammals.[6] Dysregulation of TET1 expression is closely related to various genetic diseases and cancers, such as MLL-rearranged leukaemia, hepatocellular carcinoma, gastric cancer, and breast cancer.[7] Therefore, sensitive quantification of TET1 activity is of great importance to biomedical research, clinical diagnosis, and disease therapy.

The conventional methods for TET1 assay include chromatin immunoprecipitation assay (ChIP),[8] enzyme linked immunosorbent assay (ELISA),[9] western blotting,[10] liquid-chromatography–tandem mass spectrometry (LC–MS/MS),[11] fluorescence polarization assay,[12] and electrochemical measurement.[13] However, their practical applications are limited due to the involvement of large amounts of TET1-specific antibodies,[8–10] high sample input,[10] time-consuming separation steps,[11] and unsatisfactory sensitivity.[12,13] The development of sensitive methods for antibody-free detection of TET1 is highly desirable.

Semiconductor quantum dots (QDs) exhibit the outstanding optical properties of high brightness, bleaching resistance, long fluorescence lifetimes, high quantum yields, wide absorption spectra, and narrow emission spectra,[14] making them function as promising alternatives to conventional fluorescent organic dyes in biosensing, bioimaging, and drug delivery.[15] In this research, we developed a single QD-based fluorescence resonance energy transfer (FRET) biosensor for antibody-free detection of TET1. This biosensor can sensitively detect TET1 with a low detection limit of $1.7 \times 10^{-12}$ M, and it can be applied to measure the enzymatic activity of TET1 in human neuroblastoma cells and screen TET1 inhibitors as well.

The principle of a single QD-based FRET biosensor for antibody-free detection of TET1 is illustrated in Scheme 1. We designed a Cy5/biotin-modified hairpin detection probe with one 5mC for sensing TET1. The stem region contains a 5′-C-5mC-G-G-3′/3′-G-G-C-C-5′ site which is the recognition sequence of MspI. In the presence of TET1, TET1 catalyzes the conversion of 5mC to 5hmC,[2] generating a hydroxymethylated detection probe. The T4 Phage β-glucosyltransferase (T4-βGT) can transfer the glucose moiety of uridine diphosphoglucose (UDP-glucose) to the hydroxymethyl of 5hmC, generating a glucosylated detection probe with β-glucosyl-5-hydroxymethylcytosine (5ghmC). The resultant glucosylated detection probe cannot be cleaved by the

[a] *College of Chemistry, Chemical Engineering and Materials Science, Collaborative Innovation Center of Functionalized Probes for Chemical Imaging in Universities of Shandong, Key Laboratory of Molecular and Nano Probes, Ministry of Education, Shandong Provincial Key Laboratory of Clean Production of Fine Chemicals, Shandong Normal University, Jinan 250014, China. E-mail: cyzhang@sdnu.edu.cn; Fax: +86 531-82615258; Tel: +86 531-86186033*

[b] *School of Chemistry and Chemical Engineering, Southeast University, Nanjing 211189, China*

[c] *Department of Internal Medicine, Affiliated Cancer Hospital of Zhengzhou University, Zhengzhou, Henan, China*

[d] *Academy of Medical Sciences, Zhengzhou University, Zhengzhou, Henan, 450000, China. E-mail: jiangeqiu@zzu.edu.cn*

† Electronic supplementary information (ESI) available. See DOI: 10.1039/d1cc01057c

‡ These authors contributed equally.

Published on 19 March 2021. Downloaded on 5/15/2021 9:14:33 PM.

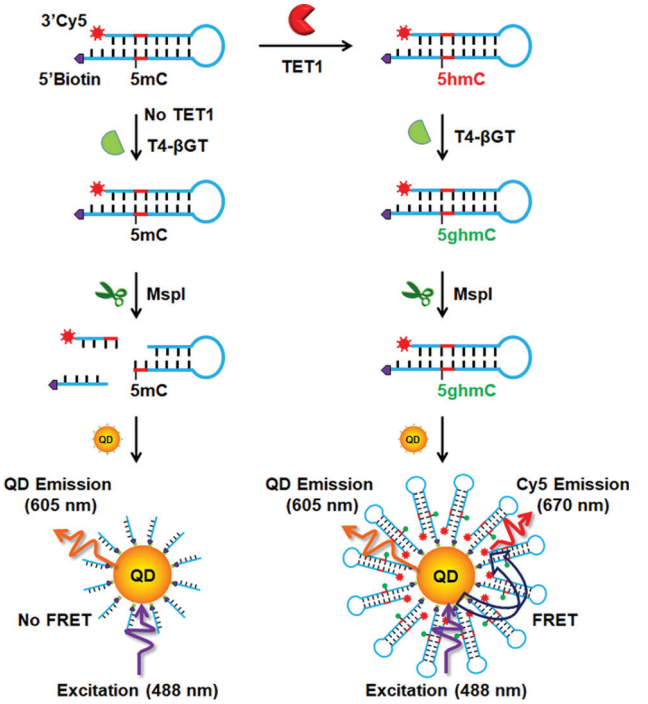


Scheme 1 Schematic illustration of a single QD-based FRET biosensor for antibody-free detection of TET1 activity.

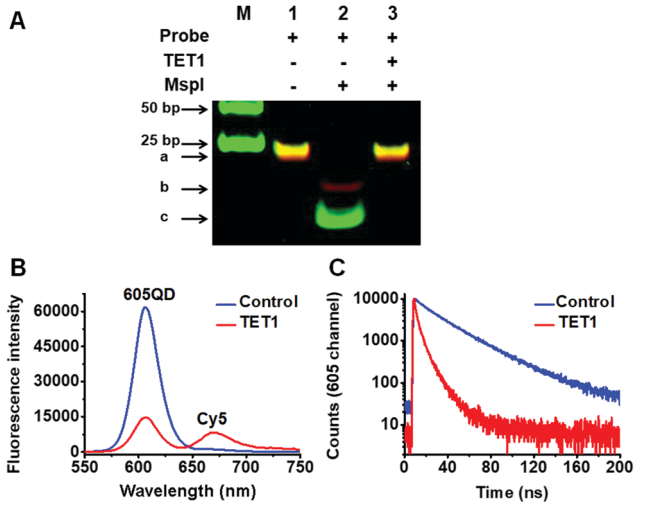


Fig. 1 (A) PAGE analysis of TET1-induced hydroxymethylation products. The signals of SYBR Gold (green) and Cy5 (red) were obtained separately, and merged into a superimposed image. The colocalization of SYBR Gold and Cy5 signals is shown in yellow. (B) Fluorescence spectral measurement of the TET1-induced QD-based FRET biosensor in the absence (blue line) and presence of TET1 (red line). (C) Fluorescence lifetime curves of the 605QD in the absence (blue line) and presence (red line) of TET1. The lifetime is measured in the emission channel of 605 nm. The TET1 concentration is 230 nM.

methylation-insensitive restriction enzyme MspI,[16] with both Cy5 and biotin being still caged in the glucosylated detection probe. Subsequently, the glycosylated Cy5/biotin-modified detection probe can assemble onto a 605 nm-emitting streptavidin-coated CdSe/ZnS QD (605QD) to obtain a 605QD-DNA-Cy5 nanostructure. Under 488 nm laser excitation, efficient FRET between the 605QD and Cy5 occurs, resulting in the emission of Cy5. The Cy5 signals can be simply counted by single-molecule detection for the quantification of TET1 activity. However, in the absence of TET1, no hydroxymethylation reaction occurs, and the 5mC remains intact. When T4-βGT is mixed with the methylated detection probe, the 5mC in the detection probe cannot undergo the glycosylation reaction, because only 5hmC can be specifically modified by T4-βGT into glucosylated 5hmC. As a result, the 5′-C-5mC-G-G-3′/3′-G-G-C-C-5′ site in the detection probe can be cleaved by MspI, generating three fragments including a Cy5-labeled DNA fragment, a biotin-labeled DNA fragment, and a hairpin DNA fragment. Consequently, no Cy5 can be assembled onto the 605QD surface, and no Cy5 signal is detected due to the lack of FRET between the 605QD and Cy5.

To determine whether TET1 can induce the hydroxymethylation of the detection probe, we performed 12% PAGE analysis (Fig. 1A and Fig. S1, see the ESI†). The PAGE results are examined by direct excitation of SYBR Gold and Cy5. In the presence of the hairpin detection probe alone, only a 35 nt band is observed (Fig. 1, lane 1, a). In the presence of MspI but without TET1, new bands of the 7 nt Cy5-labeled DNA fragment (Fig. 1A, lane 2, b) and 18 nt hairpin DNA fragment (Fig. 1A, lane 2, c) appear, suggesting the occurrence of MspI-mediated cleavage of the methylated detection probe. In the presence of both TET1 and MspI, only a 35 nt band of the glucosylated detection probe (Fig. 1A, lane 3, a) is observed, indicating that TET1 can induce the hydroxymethylation of the detection probe and MspI cannot cleave the resultant glucosylated detection probe. To verify the TET1-mediated FRET between the 605QD and Cy5, we measured the fluorescence emission spectra of the 605QD and Cy5 (Fig. 1B) and the fluorescence lifetime curves of the 605QD (Fig. 1C) in the presence and absence of TET1, respectively. The presence of TET1 induces the decrease of the 605QD fluorescence emission spectrum accompanied by the appearance and increase of the Cy5 fluorescence emission spectrum (Fig. 1B). Moreover, the presence of TET1 induces a decrease of the 605QD fluorescence lifetime (Fig. 1C). The FRET efficiency obtained by fluorescence spectral measurement is 77%, consistent with the value of 76% obtained by fluorescence lifetime measurement (see the ESI†). The high FRET efficiency can be attributed to the (1) significant 605QD emission/Cy5 absorption spectral overlap (see the ESI,† Fig. S2), (2) large Förster distance for the 605QD/Cy5 pair ($2R_0$ = 15 nm), (3) effective donor–acceptor separation distance (calculated distance of 9.2 nm based on 0.34 nm for each nucleotide in dsDNA, 1.7 nm for the distance between the Cy5 molecule and the surface of the streptavidin-coated 605QD, and 7.5 nm for the radius of the streptavidin-coated 605QD), and (4) single 605QD donor/multiple Cy5 acceptor nanostructure.

The detection of TET1 activity can be achieved by total internal reflection fluorescence (TIRF) microscopy-based single-molecule fluorescence imaging (see the ESI,† Materials and methods). As shown in Fig. 2A, only a 605QD signal is observed in the absence of TET1. In contrast, both 605QD

 This journal is © The Royal Society of Chemistry 2021

Published on 19 March 2021. Downloaded on 5/15/2021 9:14:33 PM.

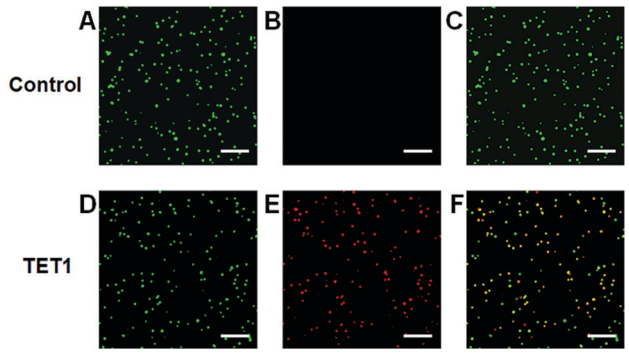


Fig. 2 (A–F) Single-molecule fluorescence images in the absence (A–C) and presence of TET1 (D–F). The 605QD fluorescence signal is shown in green (A and D), and the Cy5 fluorescence signal is shown in red (B and E). The yellow color indicates the colocalization of the 605QD and Cy5 (C and F). The TET1 concentration is 230 nM. The scale bar is 5 μm.

(Fig. 2D, green color) and Cy5 (Fig. 2E, red color) signals are simultaneously detected in the presence of TET1. Moreover, the Cy5 signal colocalizes with the 605QD signal, generating a yellow color signal (Fig. 2F). Notably, the 605QD signal in the presence of TET1 (Fig. 2D, green color) is much lower than that in the absence of TET1 (Fig. 2A, green color) due to the TET1-mediated FRET from the 605QD to Cy5. These results demonstrate that the single QD-based FRET biosensor can be used to accurately detect TET1 by simply counting the Cy5 signals.

We further investigated the sensitivity of the single QD-based FRET biosensor under optimal conditions (see the ESI,† Fig. S3 and S4). As shown in Fig. 3A, the Cy5 counts enhance with the increase of TET1 concentration from 0 to $2.3 \times 10^{-7}$ M. Moreover, the Cy5 counts are linearly dependent on the logarithm of TET1 concentration in the range from $5.0 \times 10^{-12}$ to $5.0 \times 10^{-9}$ M (inset of Fig. 3A). The equation of linear regression is $N = 5082 + 430 \log_{10} C$ ($R^2 = 0.994$), where $C$ is the TET1 concentration ($M$) and $N$ is the Cy5 counts. The detection limit is calculated to be $1.7 \times 10^{-12}$ M ($1.4 \times 10^{-7}$ μg μL$^{-1}$) based on the mean plus three times standard deviation of the control group. Notably, the sensitivity of the single QD-based FRET biosensor is enhanced by 3 orders of magnitude compared with the electrochemical biosensor ($9.8 \times 10^{-4}$ μg μL$^{-1}$).[13]

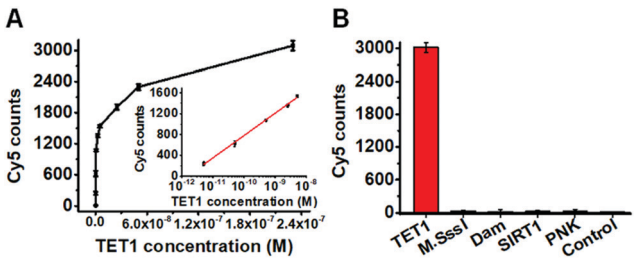


Fig. 3 (A) Variance of Cy5 counts as a function of TET1 concentration. The inset shows the linear correlation between the Cy5 counts and the logarithm of TET1 concentration. (B) Measurement of Cy5 counts in response to 230 nM TET1, 23 U mL$^{-1}$ M. SssI, 23 U mL$^{-1}$ Dam, 230 nM SIRT1, 23 U mL$^{-1}$ PNK, and the reaction buffer (control). Error bars represent standard deviations of three experiments.

We investigated the specificity of the single QD-based FRET biosensor using four nonspecific proteins including M. SssI CpG methyltransferase (M. SssI), Dam methyltransferase (Dam), sirtuin 1 deacetylase (SIRT1), and T4 polynucleotide kinase (PNK) for comparison. As shown in Fig. 3B, the nonspecific proteins only generate negligible responses. In contrast, the presence of TET1 generates high Cy5 counts, and the signal in response to TET1 is 85-fold, 131-fold, 119-fold, and 80-fold higher than those in response to M. SssI, Dam, SIRT1, and PNK, respectively, suggesting the high specificity of the single QD-based FRET biosensor toward TET1.

We further investigated whether this single QD-based FRET biosensor can be used for the screening of potential TET1 inhibitors. TET1 belongs to the Fe(II)- and 2-oxoglutarate-dependent dioxygenase family which is highly sensitive to nickel inhibition.[17] We used the nickel (Ni(II)) ion as the TET1 model inhibitor. The Ni(II) ion may displace the cofactor Fe(II) to directly bind with the Fe-binding site of TET1, leading to a dysfunction of TET1-mediated 5mC oxidation activity. As shown in Fig. 4, the value of $IC_{50}$ is estimated to be 3.3 μM based on the curve of relative activity *versus* the inhibitor concentration. The obtained $IC_{50}$ value is consistent with that obtained by the UHPLC-MS/MS analysis (1.2 μM).[17] In addition, this single QD-based FRET biosensor can be used to detect the kinetic parameters of TET1 (see the ESI,† Fig. S5). The $K_m$ value is estimated to be 0.46 ± 0.054 μM and $K_{cat}$ is calculated to be $(1.6 \pm 0.080) \times 10^{-4}$ s$^{-1}$, consistent with the values obtained by LC-MS/MS assay ($K_m$ = 0.38 ± 0.10 μM and $K_{cat}$ = $(6.0 \pm 0.55) \times 10^{-4}$ s$^{-1}$),[18] suggesting that this single QD-based FRET biosensor can be used to accurately evaluate the kinetic parameters of TET1.

We used a human tumorigenic N-type neuroblastoma cell line (SK-N-BE(2) cells) and a human cervical carcinoma cell line (HeLa cells) as the models to demonstrate the feasibility of the single QD-based FRET biosensor for cellular TET1 activity assay. After cell extraction, the resultant supernatant was subjected to TET1 assay, with different dilutions of cell lysates being used for cellular TET1 assay and linear relationship analysis (see the ESI,† Materials and methods). No significant signal is detected in HeLa cells (Fig. 5A, green column) compared with that obtained in the control group with only reaction buffer (Fig. 5A, blue column), suggesting no TET1

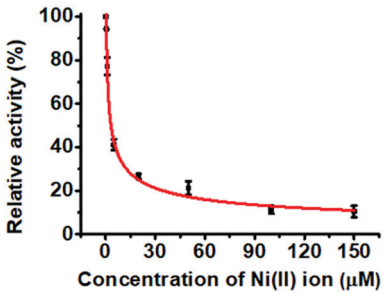


Fig. 4 Measured relative activity of TET1 as a function of the Ni(II) ion concentration for enzyme inhibitor analysis. The TET1 concentration is 230 nM. Error bars represent standard deviations of three experiments.

Published on 19 March 2021. Downloaded on 5/15/2021 9:14:33 PM.

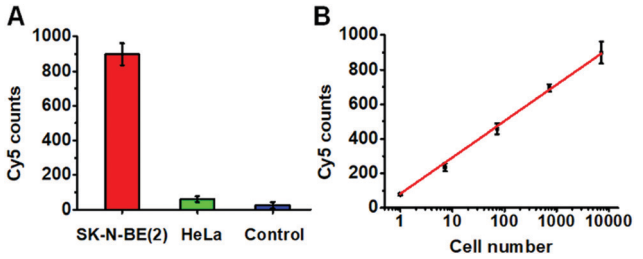


Fig. 5 (A) Variance of Cy5 count in response to cellular extracts (equivalent to 7200 cells) from SK-N-BE(2) cells (red column), HeLa cells (green column), and the reaction buffer (control, blue column). (B) Logarithmic dependence of the Cy5 counts on the number of SK-N-BE(2) cells in the range from 1 to 7200 cells. Error bars represent standard deviations of three experiments.

expression in HeLa cells, consistent with previous research.[19] In contrast, a higher Cy5 signal is detected in SK-N-BE(2) cells (Fig. 5A, red column); it is 15-fold higher than that detected in HeLa cells, suggesting the high expression of TET1 in SK-N-BE(2) cells, consistent with the results obtained by real-time quantitative polymerase chain reaction (RT-qPCR) analysis[19b] and a capillary electrophoresis with laser-induced fluorescence detection (CE-LIF) method.[19c] We further investigated the relationship between the Cy5 counts and the number of SK-N-BE(2) cells. The Cy5 counts enhance with the increase of the number of SK-N-BE(2) cells (Fig. 5B). In the logarithmic scale, there is a linear relationship between the Cy5 counts and the number of SK-N-BE(2) cells in the range of 1 − 7200. The correlation equation is $N = 82 + 210 \log_{10} X$ ($R^2 = 0.998$), where $X$ is the number of SK-N-BE(2) cells and $N$ is the Cy5 counts. The detection limit is 1 cell.

In summary, we have developed a single QD-based FRET biosensor for antibody-free detection of TET1. In comparison with previously reported antibody-based methods,[8–10] this single QD-based FRET biosensor does not involve large amounts of TET1-specific antibodies, high sample input, and time-consuming separation steps. Due to the specific TET1-mediated hydroxymethylation and glycosylation, the TET1-mediated high FRET efficiency from the 605QD to Cy5, and the high signal-to-noise ratio of single-molecule detection, this single QD-based FRET biosensor can achieve high sensitivity with a detection limit of $1.7 \times 10^{-12}$ M. Importantly, this single QD-based FRET biosensor can be used to accurately measure TET1 activity in cancer cells with a detection limit of 1 cell, and it can be further applied for the screening of TET1 inhibitors, providing a new platform for clinical diagnosis and drug discovery.

This work was supported by the National Natural Science Foundation of China (Grant No. 21735003), and the Award for Team Leader Program of Taishan Scholars of Shandong Province, China.

## Conflicts of interest

There are no conflicts to declare.

## Notes and references

1 (*a*) P. W. Hill, R. Amouroux and P. Hajkova, *Genomics*, 2014, **104**, 324–333; (*b*) R. Métivier, R. Gallais, C. Tiffoche, C. Le Péron, R. Z. Jurkowska, R. P. Carmouche, D. Ibberson, P. Barath, F. Demay, G. Reid, V. Benes, A. Jeltsch, F. Gannon and G. Salbert, *Nature*, 2008, **452**, 45–50; (*c*) B. Yao, K. M. Christian, C. He, P. Jin, G. L. Ming and H. Song, *Nat. Rev. Neurosci.*, 2016, **17**, 537–549; (*d*) M. M. Dawlaty, A. Breiling, T. Le, M. I. Barrasa, G. Raddatz, Q. Gao, B. E. Powell, A. W. Cheng, K. F. Faull, F. Lyko and R. Jaenisch, *Dev. Cell*, 2014, **29**, 102–111.
2 M. Tahiliani, K. P. Koh, Y. Shen, W. A. Pastor, H. Bandukwala, Y. Brudno, S. Agarwal, L. M. Iyer, D. R. Liu, L. Aravind and A. Rao, *Science*, 2009, **324**, 930–935.
3 S. Ito, A. C. D'Alessio, O. V. Taranova, K. Hong, L. C. Sowers and Y. Zhang, *Nature*, 2010, **466**, 1129–1133.
4 R. M. Kohli and Y. Zhang, *Nature*, 2013, **502**, 472–479.
5 Y. F. He, B. Z. Li, Z. Li, P. Liu, Y. Wang, Q. Tang, J. Ding, Y. Jia, Z. Chen, L. Li, Y. Sun, X. Li, Q. Dai, C. X. Song, K. Zhang, C. He and G. L. Xu, *Science*, 2011, **333**, 1303–1307.
6 J. U. Guo, Y. Su, C. Zhong, G. L. Ming and H. Song, *Cell*, 2011, **145**, 423–434.
7 (*a*) R. B. Lorsbach, J. Moore, S. Mathew, S. C. Raimondi, S. T. Mukatira and J. R. Downing, *Leukemia*, 2003, **17**, 637–641; (*b*) C. Liu, L. Liu, X. Chen, J. Shen, J. Shan, Y. Xu, Z. Yang, L. Wu, F. Xia, P. Bie, Y. Cui, X. W. Bian and C. Qian, *PLoS One*, 2013, **8**, e62828; (*c*) Y. F. Pei, R. Tao, J. F. Li, L. P. Su, B. Q. Yu, X. Y. Wu, M. Yan, Q. L. Gu, Z. G. Zhu and B. Y. Liu, *Oncotarget*, 2016, **7**, 31322–31335; (*d*) C. R. Good, S. Panjarian, A. D. Kelly, J. Madzo, B. Patel, J. Jelinek and J. J. Issa, *Cancer Res.*, 2018, **78**, 4126–4137.
8 J. Xiong, Z. Zhang, J. Chen, H. Huang, Y. Xu, X. Ding, Y. Zheng, R. Nishinakamura, G. L. Xu, H. Wang, S. Chen, S. Gao and B. Zhu, *Mol. Cell*, 2016, **64**, 913–925.
9 D. Nettersheim, L. C. Heukamp, F. Fronhoffs, M. J. Grewe, N. Haas, A. Waha, F. Honecker, A. Waha, G. Kristiansen and H. Schorle, *PLoS One*, 2013, **8**, e82881.
10 B. Thienpont, J. Steinbacher, H. Zhao, F. D'Anna, A. Kuchnio, A. Ploumakis, B. Ghesquière, L. Van Dyck, B. Boeckx, L. Schoonjans, E. Hermans, F. Amant, V. N. Kristensen, K. Peng Koh, M. Mazzone, M. Coleman, T. Carell, P. Carmeliet and D. Lambrechts, *Nature*, 2016, **537**, 63–68.
11 L. Hu, J. Lu, J. Cheng, Q. Rao, Z. Li, H. Hou, Z. Lou, L. Zhang, W. Li, W. Gong, M. Liu, C. Sun, X. Yin, J. Li, X. Tan, P. Wang, Y. Wang, D. Fang, Q. Cui, P. Yang, C. He, H. Jiang, C. Luo and Y. Xu, *Nature*, 2015, **527**, 118–122.
12 L. J. Marholz, W. Wang, Y. Zheng and X. Wang, *ACS Med. Chem. Lett.*, 2016, **7**, 167–171.
13 Z. Yu, X. Chen, Y. Cheng, H. Yang, F. Wang and Z. Chen, *Anal. Chim. Acta*, 2021, **1146**, 140–145.
14 P. Alivisatos, *Nat. Biotechnol.*, 2004, **22**, 47–52.
15 (*a*) W. R. Algar, K. Susumu, J. B. Delehanty and I. L. Medintz, *Anal. Chem.*, 2011, **83**, 8826–8837; (*b*) Y. Yang, M. Xia, S. Zhang and X. Zhang, *Chem. Commun.*, 2019, **56**, 145–148; (*c*) T. Yu, D. M. Wei, Z. Li, L. J. Pan, Z. L. Zhang, Z. Q. Tian and Z. Liu, *Chem. Commun.*, 2020, **56**, 1976–1979; (*d*) C.-C. Li, W.-X. Liu, J. Hu and C.-Y. Zhang, *Chem. Sci.*, 2019, **10**, 8675–8684.
16 C. Zhao, H. Wang, B. Zhao, C. Li, R. Yin, M. Song, B. Liu, Z. Liu and G. Jiang, *Nucleic Acids Res.*, 2014, **42**, e81.
17 R. Yin, J. Mo, J. Dai and H. Wang, *ACS Chem. Biol.*, 2017, **12**, 1494–1498.
18 L. Liang, J. Chen, Y. Li, X. Lai, H. Sun, C. Li, M. Zhang, T. Yang, F. Meng, P. Y. Law, H. H. Loh and H. Zheng, *Cell Rep.*, 2020, **30**, 3625–3631.
19 (*a*) A. Ramsawhook, L. Lewis, B. Coyle and A. Ruzov, *Clin. Epigenetics*, 2017, **9**, 18; (*b*) C. J. Mariani, A. Vasanthakumar, J. Madzo, A. Yesilkanal, T. Bhagat, Y. Yu, S. Bhattacharyya, R. H. Wenger, S. L. Cohn, J. Nanduri, A. Verma, N. R. Prabhakar and L. A. Godley, *Cell Rep.*, 2014, **7**, 1343–1352; (*c*) A. M. Krais, Y. J. Park, C. Plass and H. H. Schmeiser, *Epigenetics*, 2011, **6**, 560–565.

 This journal is © The Royal Society of Chemistry 2021